SLAC-PUB-9991
June 2003

High Anisotropy CoPtCrB Magnetic Recording Media

Michael F. Toney *et al.*

Submitted to Journal of Applied Physics

Stanford Linear Accelerator Center, Stanford University, Stanford, CA 94309

Work supported by Department of Energy contract DE–AC03–76SF00515.

High Anisotropy CoPtCrB Magnetic Recording Media

Michael F. Toney [a],* Ernesto E. Marinero, Mary F. Doerner and Philip M. Rice

IBM Almaden Research Center

IBM Research Division

650 Harry Road

San Jose, Ca 95120

(Dated: June 16, 2003)

Abstract

We describe the synthesis, magnetism and structure of CoPtCrB alloys with Pt concentrations from 10 - 43 %. The Cr concentration in the alloys was 15-17 % and the B concentration was 9-11 %. The magnetic anisotropy and coercivity increase with increasing Pt up to $\approx$ 30%, plateau at $\approx$ 35,000 Oe and $\approx$ 6000 Oe, respectively, and then decrease. Transmission electron microscopy results show the media form fine, isolated grains for all Pt concentrations. X-ray diffraction measurements show that with increasing Pt an fcc Co-alloy phase is progressively formed at the expense of the hcp Co-alloy and that this fraction becomes significant for $>$ 35% Pt. The formation of the fcc phase likely causes the behavior in the anisotropy. No Pt concentration dependence is observed for the stacking fault density. The X-ray data show that with increasing Pt the CoPtCrB alloy lattice parameters exhibit two distinct regions with the slope changing at 16 % Pt. The presence of these two regions is discussed.

PACS numbers: 75.50.SS, 75.30.Gw, 61.72.Dd, 68.55.Jk

*Electronic address: mftoney@slac.stanford.edu

I. INTRODUCTION

The development of thermally stable, thin, small grain recording media is pivotal for magnetic recording beyond 200 Gbits/in^2. This requires media with high magnetic anisotropy and coercivity [1]. There are several alternative materials under investigation that provide adequately high anisotropy, including chemically ordered $L1_0$ alloys such as FePt and CoPt [2, 3] and rare-earth transition-metal alloys [4, 5]. Another route to achieve this goal is to increase the magnetocrystalline anisotropy of current state-of-the-art CoPtCrB alloys [6]. The anisotropy is enhanced by Pt substitution of the Co atoms in the hexagonal-close packed (hcp) structure. This approach has the advantage that it is a relatively small change in the disk manufacturing process.

Previous work on high Pt concentrations in media have included CoPt alloys [7–11], CoPtCr and CoCrTa alloys [12–15] and a little reported work on CoPtCrB [6]. The general trend for these has been an initial increase in the coercivity (H_c) and anisotropy with increasing Pt, followed by a plateau and then a decrease in H_c. However, the Pt concentration where H_c begins to plateau and drop varies from study to study. This dependence of H_c on Pt concentration has been suggested to arise from a variety of mechanisms, including an increase in grain size [8, 9], the formation of stacking faults [12, 13], the formation of face-centered cubic (fcc) grains [11], and an improvement in crystal quality [6]. Note that both the empirical bulk phase diagram for Co-Pt [16] and the calculated phase diagram for Co-Pt-Cr [17] are incomplete for low Pt concentrations at low temperatures. However, these suggest that hcp CoPt transforms in fcc CoPt around 15-25% Pt. While the bulk phase diagram is not necessarily pertinent to thin films, this suggests that the increasing presence of an fcc CoPt alloy with increasing Pt may play a role in affecting the magnetic properties.

In this paper, we describe CoPtCrB alloys with Pt concentrations varying from 10-43 %, while the Cr content was fixed at 15-17 % and the B content at 9-11 %. These alloys exhibit $H_c \approx 6000$ Oe and anisotropy fields (H_k) $\approx$ 30,000 Oe. We find that the anisotropy linearly increases with Pt up to $\approx$ 30 %, then peaks for Pt between 30 and $\approx$ 35 % and finally decreases with added Pt concentrations. Transmission electron microscopy (TEM) on these media show that the magnetic grains are segregated by a secondary (presumably non-magnetic) phase. X-ray diffraction measurements show that with increasing Pt incorporation in the alloy an fcc alloy phase is progressively formed at the expense of the hcp alloy and that

the fcc fraction becomes significantly large for >35% Pt. Because fcc Co has a much lower anisotropy than hcp Co, this observation shows that the formation of the fcc CoPtCrB phase results in the Pt concentration dependence observed for the CoPtCrB anisotropy. There is no Pt concentration dependence to the stacking fault density. The X-ray data also show that with increasing Pt the CoPtCrB alloy lattice parameters increase nonlinearly, which may be related to the fcc alloy formation.

II. EXPERIMENTAL ASPECTS

Thin film disks were deposited by dc magnetron sputtering using a Balzers Process System Circulus M12 system. The deposition temperature was 260 - 280 deg C and the base pressure was approximately 2×10^{-7} Torr. We have investigated media grown with several different preferred orientations obtained using different seed and underlayers on both glass and metal substrates. These include:

A. glass/NiAl/CrV/CoCr/CoPtCrB/C with a $(10\bar{1}0)$ preferred orientation, including the media described in Ref. 18.

B. NiP/NiAl/Cr/CoCr/CoPtCrB/C with a $(10\bar{1}0)$ preferred orientation.

C. glass/seedlayer/CrMo/CoCr/CoPtCrB/C with a $(11\bar{2}0)$ preferred orientation [19].

D. NiP/RuAl/CrMo/CoCr/CoPtCrB/C with a $(11\bar{2}0)$ preferred orientation.

In all cases, the media thickness was 10-20 nm. The Cr composition was typically 15-17 %, while the B compostion was 9-11 %.

A vibrating sample magnetometer (VSM) and a remanence magnetometer (RMM) were used to determine H_c, saturation magnetization (M_s) and coercive squareness (S*). H_k measurements were conducted by determining the field required to fully orient the magnetization along the hard axis. Both the VSM and a Kerr technique were employed for this purpose. Independent measurements of the magnetization and the film dimensions allow one to calculate the maximum H_k per grain and these are the values reported below. Thermal decay measurements were conducted employing the coercivity dependence on switching speed and the data were analyzed utilizing the Sharrock model [20].

To create TEM specimens, a section was cut from each disk and the back was ground away to expose the AlMg substrate. The AlMg was etched away using a Sodium Hydroxide solution. A hole punch was used to punch out 3 mm circles which were then glued to 50

micron thick Mo aperture grids. The specimens were then Ar ion milled to perforation from the back side of the specimen. The TEM images were acquired using a TopCon 002B operating at 110 kV equipped with a CCD camera.

X-ray scattering data were collected at the National Synchrotron Light Source, Brookhaven National Laboratory, beamline X20, with a focused X-ray beam. Several experimental runs were used to collect the complete data set, and in all these runs an incident X-ray energy of about 10.3 keV (wavelength of about 1.2 Å) was used. When possible, diffuse scattering from the substrate was minimized by using a grazing incidence geometry. The diffracted beam was analyzed with 1 milliradian (mrad) Soller slits and the acceptance out of the scattering plane was about 15 mrad. A Ge detector was used to discriminate the elastic scattering from the Co, Cr, and Ni fluorescence.

In the discussion below, the scattering vector **Q** is the vector difference between the incoming and diffracted X-rays. It has a magnitude given by $Q = (4\pi/\lambda) \sin\theta$; we will resolve **Q** into components parallel and perpendicular to the disk surface, Q_x and Q_z, respectively. The angle that **Q** makes to the surface normal is then $\chi = \arccos(Q_z/Q)$.

III. MAGNETIC RESULTS

Figures 1 (a) and (b) show H_c and H_k as a function of Pt concentration for type A disks. Present media have $H_c \approx 4$ kOe and $H_k \approx 20$ kOe [19], while H_k for pure, bulk Co is 6.4 kOe [21]. As is evident, H_k increases nearly linearly up to about 30 % Pt then plateaus and finally drops above about 40 % Pt; H_c follows a similar trend. This flattening and then dropping in H_c has been observed before in CoPtCr media [11, 13, 15], but, in these studies, H_c began to plateau at much lower Pt concentration ($\approx$ 10-15 % Pt). The reasons for this difference are not completely clear. One possibility is our use of CoPtCrB rather CoPtCr. In CoPtCr, the Cr quenches the moment, while in CoPtCrB, assuming that more of the Cr segregates to the grain boundary phase [22], the Cr will have a smaller effect on the moment. Another possibility is that there is less fcc phase in CoPtCrB than in CoPtCr [23], which is reasonable, because some B is incorporated interstitially in the media and the hcp has larger interstitial sites. This may tend to stabilize the hcp phase. Alternatively, this difference in the concentration where H_c reaches a plateau could be due to the use of different underlayers [11, 14], or to different growth conditions. The thermal

decay rate of our CoPtCrB media decreases with increasing Pt (from about 15%/decade to $\approx$ 1%/decade), consistent with the increase in H_k. The behavior of saturation magnetization (M_s) with Pt concentration is shown in Fig. 1(c) for type A media. There is a monotonic decrease in M_s with increasing Pt, consistent with previous results on CoPt [8, 24] and CoPtCr alloys [13, 15]. This behavior is probably due to both a simple dilution of Pt for Co and a lowering of the Co-alloy Curie temperature. The coercivity squareness is about 0.9, nearly independent of Pt concentration.

IV. STRUCTURAL RESULTS

For each disk, X-ray diffraction measurements were done to determine the lattice parameters, the film texture, the stacking fault densities and the fraction of fcc regions in the media. The in-plane lattice parameters were obtained from in-plane diffraction scans, $Q_z \simeq 0$ (see Fig. 2). The stacking fault (growth and deformation) were determined from the widths of the $(10\bar{1}1)$, $(10\bar{1}2)$ and $(10\bar{1}3)$ peaks, after accounting for grain size and non-uniform strain [25, 26]. These peaks were measured in radial scans with χ such that the scans went through the maximum in the peak (see Fig. 2). Note that for $(11\bar{2}0)$ preferred orientation, these included in-plane scans.

To determine the fcc concentration, radial diffraction scans were taken through the fcc(200) and hcp$(10\bar{1}1)$ peaks. The values of χ for these depended on the preferred media orientation, as illustrated in Figure 2 for media with both $(10\bar{1}0)$ and $(11\bar{2}0)$ preferred orientations, (a) and (b), respectively. To minimize the diffraction from the underlayers and the glass substrates, these data were obtained with a grazing incidence angle (typically 0.3 deg). An example of scans through the fcc(200) and hcp$(10\bar{1}1)$ peaks are shown in Figure 3 for $(10\bar{1}0)$ media with 10, 17, 36 and 41 % Pt (media type A and B). As is evident, the intensity of the fcc(200) peak, and hence the amount of fcc CoPtCrB alloy, increases significantly with increasing Pt concentration. The fcc concentration was quantified from the integrated intensity of the fcc(200) peak to that of the hcp$(10\bar{1}1)$ peak taking into account the multiplicity, form factor, Lorentz-polarization factor, and Debye-Waller factor [25]. Since x-ray diffraction is volume averaging, we cannot determine if the fcc regions form isolated grains or are intra-granular.

As shown before [19], the extent of preferred orientation is quite different for $(10\bar{1}0)$ and

$(11\bar{2}0)$ oriented media. This is a result of the large difference in the extent of preferred orientation in the seed and underlayers. However, for a given media orientation, we have found no systematic dependence in the extent of preferred orientation on the Pt concentration, which is reasonable given that this is determined largely by the seed and underlayers.

The a and c in-plane lattice parameters of the various media are shown in Fig. 4 as a function of Pt concentration. In addition to data obtained from this study, data from previous investigations [15, 27] have been included. The solid lines are guides to the eye; the dashed and dot-dashed lines are the lattice parameters calculated using Vegard's law (linear extrapolation between Co and Pt) and using an elastic model due to Friedel (valid only at low concentrations), respectively [28, 29]. In both cases, these models are for hcp Co-Pt solid solutions and ignore the Cr and B. While these approximations are not expected to be accurate, they do provide guides. In addition, there are no bulk data (even for Co-Pt) to compare with Fig. 4. Several important trends are evident in the data in Fig. 4. First, there are two distinct linear ranges in the data: a low Pt region from 0 - 16 % Pt and a high Pt region from 16 - 45 % Pt. These regions have significantly different slopes. We do not fully understand the presence of these two regions, but it may be related to the initial formation of fcc CoPtCrB alloy, which begins near 15% Pt (see below). Second, there is no significant dependence of either a or c on the preferred orientation, although there is a small dependence [30]. Last, as expected, Vegard's law underestimates the lattice parameters, while Friedel's approximation provides a more accurate prediction of the trends [28]. Some of the discrepancy between these models and the data is likely due to ignoring the B and, perhaps, the Cr in the alloys.

Figure 5(a) shows the fraction of fcc CoPtCrB alloy in the otherwise hcp media. From these data, it is apparent that the fcc fraction is approximately linear until about 35% Pt. Above this Pt concentration, the fcc fraction increases more quickly. These data are compared with the H_c and H_k in the following section. It is important to note that we have carefully searched for the chemically ordered, hexagonal DO_{19} Co_3Pt phase [1, 31], but have found absolutely no evidence for this.

The stacking fault densities are shown in Figure 5(b) and (c) as a function of Pt concentration. For all Pt concentrations studied, both the growth and deformation fault densities do not show a significant trend with Pt concentration, except perhaps for a slight increase in the growth faults above about 35% Pt. The lack of increase in fault density with Pt

concentration is rather surprising, since high concentration of faults are found in Co-alloys near the fcc-hcp transition region [32]. This may be a result of segregation of Pt into the fcc regions, which would be consistent with the decrease in nonuniform strain with increasing Pt concentration (see Fig. 6). The magnitude of the fault densities in Fig. 5 are consistent with those found by TEM in CoPtCr media [12].

Figure 6 shows the non-uniform strain and the particle size for the CoPtCrB media as a function of Pt concentration. The non-uniform strain is the root-mean-square variation in lattice parameter through the media grains, normalized to the average lattice parameter. The non-uniform strain and the particle size were determined by the diffraction peak widths using the method of integral breadths [25]. As is apparent in Fig. 6(a), the non-uniform strain decreases significantly (nearly a factor of two) from 10 to 40 % Pt. Since Pt is much larger than Cr and Co, this trend is opposite to that one might expect if the media were a uniform alloy. While the cause of the decrease is not entirely clear, this could be a result of the change in Cr and/or B segregation to the grain boundaries as the Pt concentration changes [6, 15]. Less segregation could lead to a more homogeneous crystalline grain and hence less non-uniform strain. Figure 6(b) shows that the particle size (related to grain size) increases slightly with Pt concentration. However, this increase is small and is probably not a significant factor affecting the VSM coercivity.

Figure 7 shows a representative TEM micrograph of the media with 32 % Pt (media type C). As is apparent, even for these high Pt concentration, the physical grains are still well isolated. The average grain size is about 8 nm, consistent with the X-ray diffraction results shown in Fig. 6(b).

V. DISCUSSION

One very simple approach to correlate the anisotropy field to the media microstructure is to assume that all the anisotropy comes from the hcp fraction of the film; the fcc part of the film does not contribute to the anisotropy. This is quite reasonable since H_k for hcp Co is more than ten times larger than for fcc Co (6.4 kOe compared to 0.6 kOe). In this simple approach, we assume that H_k depends linearly on the volume fraction of the hcp CoPtCrB phase. We also assume that any Pt grain boundary segregation does not depend significantly on Pt concentration, which seems reasonable since there is not much Pt segregation. Figure

8 plots H_k as a function of the Pt concentration times the fraction of CoPtCrB alloy that is hcp (obtained from Fig. 5). Note in this plot disks with high Pt concentration are shifted toward the left compared with Fig. 1(a). As can be seen, a linear correlation is obtained up to nearly 30 % Pt. However, the highest Pt concentration (43 % Pt) falls well off this line. This suggests that a collective effect, such as percolation of the fcc regions throughout the media, may be responsible for the low H_k in this film.

Modeling has been done to investigate how the presence of fcc grains in an otherwise hcp media thin film affects the magnetic and recording properties [33, 34]. The media were modeled as bulk Co and the media grains were either entirely fcc or hcp. These simulations found that with increasing fcc concentrations H_c decreased and that this decrease was stronger for media with smaller inter-granular exchange coupling. These conclusions are consistent with our results, particularly since the high B concentration results in small exchange coupling. It is not, however, possible to directly compare our results with the simulations, since empirically some (or all) of the fcc regions may be intra-granular.

While our general observations on the behavior of H_k and H_c with increasing Pt are qualitatively consistent with previous work [6–15], quantitatively there are significant differences in the Pt concentration where H_c plateaus and then starts to drop. This is likely a result of differences in the media alloy compositions (our use of B containing media, which prevents the Cr from effectively quenching the magnetic moment or stabilizes the hcp phase); the use of different growth conditions and seed and underlayers may also contribute to this. The mechanism leading to the H_k and H_c behavior has been suggested to originate from an increase in grain size [6, 8, 9], stacking fault formation [12, 13], or fcc-phase formation [11]. Our data show that, for the media we have produced, the fcc formation is the dominant factor; the grain growth is small and there is no change in stacking fault density with increasing Pt. This apparent discrepancy is, again, likely due to different media compositions, growth conditions, seed/underlayers, as well as different Pt concentration regimes. It is indeed surprising that we do not observe any change in stacking fault density while the amount of the fcc phase increases, since the formation of stacking faults is one mechanism for transforming hcp into fcc [26, 31]. This may be a result of the fast sputter deposition of these alloys kinetically limiting equilibrium. Finally, dependence of fcc Co-alloy on Pt concentration is qualitatively consistent with the extrapolated bulk phase diagram for Co-Pt [16].

VI. SUMMARY

We have shown that in modern CoPtCrB media the magnetic anisotropy increases with increasing Pt, plateaus and then decreases, and that this behavior is due to the formation of fcc CoPtCrB alloy in the hcp media. This can be simply understood by considering the amount of Pt in the hcp CoPtCrB alloy (Fig. 8). We do not observe an increase in stacking fault density with increasing Pt, different from observations on CoPtCr alloys [12, 13]. There are two distinct regions in the lattice parameter vs Pt data, which may be related to the initial formation of fcc CoPtCrB alloy. With increasing Pt, the media particle size increases slightly, while the nonuniform strain decreases significantly, thereby signaling changes in the grain boundary segregation.

Acknowledgments

We acknowledge the assistance of Jonathan Hedstrom in data analysis. Research carried out in part at the National Synchrotron Light Source, Brookhaven National Laboratory, which is supported by the U.S. Department of Energy, Division of Materials Sciences and Division of Chemical Sciences, under Contract No. DE-AC02-98CH10886.

VII. REFERENCES

---

[a] Permanent Address: Stanford Synchrotron Radiation Laboratory, Stanford Linear Accelerator Center, Menlo Park, CA 94025

[1] D. Weller, A. Moser, L. Folks, M. E. Best, W. Lee, M. F. Toney, M. Schwickert, J.-U. Thiele, and M. F. Doerner, IEEE Trans. Magn. **36**, 10 (2000).

[2] A. Cebollada, R. F. C. Farrow, and M. F. Toney, in *Magnetic Nanostructures*, edited by H. S. Nalwa (American Scientific, Stevenson Ranch, Ca, 2002), p. 93.

[3] K. R. Coffey, M. A. Parker, and J. K. Howard, IEEE Trans. Magn. **31**, 2737 (1995).

[4] P. I. Williams and P. J. Gundy, J. Phys. D **27**, 897 (1994).

[5] C. Prados, E. Marinero, and A. Hernando, J. Magn. Magn. Mater. **165**, 414 (1997).

[6] M. Mikami, D. D. Djayaprawira, H. Domon, S. Yoshimura, M. Takahashi, and K. Komiyama, J. Appl. Phys. **91**, 7074 (2002).

[7] J. A. Aboaf, S. R. Herd, and E. Klokholm, IEEE Trans. Magn. **19**, 1514 (1983).

[8] M. Kitada and N. Shimizu, J. Appl. Phys. **54**, 7089 (1984).

[9] T. ishiguro and J. Sato, Mat. Trans. JIM **35**, 319 (1994).

[10] J.-J. Delaunay, T. Hayashi, M. Tomita, and S. Hirono, IEEE Trans. Magn. **34**, 1627 (1998).

[11] H. Ohmori and A. Maesaka, J. Appl. Phys. **91**, 8635 (2002).

[12] A. Ishikawa and R. Sinclair, IEEE Trans. Magn. **32**, 3605 (1996).

[13] A. Ishikawa and R. Sinclair, J. Magn. Magn. Mater. **152**, 265 (1996).

[14] H.-S. Lee, D. E. Laughlin, and J. A. Bain, J. Appl. Phys. **91**, 7065 (2002).

[15] C. R. Paik, I. Suzuki, M. Ishikawa, Y. Ota, and K. Nakamura, IEEE Trans. Magn. **28**, 3084 (1992).

[16] M. Hansen, *Constitution of Binary Alloys, 2nd ed.* (McGraw-Hill, New York, 1958).

[17] K. Oikawa, G. W. Qin, T. Ikeshoji, O. Kitakami, Y. Shimada, K. Ishida, and K. Fukamichi, J. Magn. Magn. Mater. **236**, 220 (2001).

[18] J. Li, M. Mirzamaani, X. Bian, M. Doerner, S. Duan, K. Tang, M. Toney, T. Arnoldussen, and M. Madison, J. Appl. Phys. **85**, 4286 (1999).

[19] M. F. Doerner et al., IEEE Trans. Magn. **37**, 1052 (2001).

[20] M. P. Sharrock, J. Appl. Phys. **76**, 6413 (1994).

[21] B. D. Cullity, *Introduction to Magnetic Materials* (Addison-Wesley, Reading, MA, 1972).

[22] E. M. Marinero, unpublished.

[23] S. McKinlay, M. F. Doerner, unpublished.

[24] D. Weller, H. Brandle, and C. Chappert, J. Magn. Magn. Mater. **121**, 461 (1993).

[25] B. E. Warren, *X-ray Diffraction* (Addison-Wesley, Reading, MA, 1969).

[26] P. Dova, H. Laidler, K. O'Grady, M. F. Toney, and M. F. Doerner, J. Appl. Phys. **85**, 2775 (1999).

[27] M. F. Doerner, private communication.

[28] T. B. Massalski, in *Physical Metallurgy*, edited by R. W. Cahn and P. Hansen (North-Holland, Amsterdam, 1983), vol. 1, pp. 623–744.

[29] J. Friedel, Phil. Mag. **46**, 514 (1955).

[30] M. F. Toney and M. F. Doerner, unpublished.

[31] G. R. Harp, D. Weller, T. A. Rabedeau, R. F. C. Farrow, and M. F. Toney, Phys. Rev. Lett. **71**, 2493 (1993).

[32] M. T. Sebastian and P. Krishna, *Random, Non-Random and Periodic Faulting in Crystals* (Gordon and Breach, Amsterdam, 1994).

[33] K. O'Grady, N. S. Walmsley, C. F. Wood, and R. W. Chantrell, IEEE Trans. Magn. **34**, 1579 (1998).

[34] N. S. Walmsley, R. W. Chantrell, and K. O'Grady, J. Magn. Magn. Mater. **193**, 420 (1999).

VIII. FIGURE CAPTIONS

Figure 1. Anisotropy field (H_k), coercivity (H_c) and saturation magnetization (M_s) as function of Pt concentration in (a), (b) and (c), respectively. Data for the CoPtCrB media are in the open symbols and that for bulk Co is given by the filled circle. These are for media series A.

Figure 2. Diffraction peak positions for both hcp and fcc phases for (a) $(10\bar{1}0)$ and (b) $(11\bar{2}0)$ preferred orientations. This is a reciprocal space map (in Q_x and Q_z space) of the peak positions. The solid lines show some of the diffraction scans that were performed; χ is the angle that **Q** makes with the surface normal in these scans. The relative orientation between the fcc and hcp phases is that from the Shoji-Nishiyama relation.

Figure 3. Radial diffraction scans for several $(10\bar{1}0)$ oriented media (type A and B) with varying Pt concentration. These data were obtained at $\chi = 60$ deg to go through the fcc(200) and hcp$(10\bar{1}1)$ peaks as shown in Figure 2. To facilitate comparison, the intensity is plotted relative to the position of the hcp$(10\bar{1}1)$ peak (Q_B), the background scattering has been subtracted, and the intensities have been corrected for illuminated area and normalized to the peak intensity of hcp$(10\bar{1}1)$ peak. The hcp $(10\bar{1}1)$ and fcc(002) peaks are marked. The peak near $Q - Q_B$ of -0.2 Å^{-1} is the media fcc(111) diffraction overlapping with the under/seed layer (110) diffraction, while that near -0.4 Å^{-1} is the hcp$(10\bar{1}0)$.

Figure 4. Media lattice parameters as a function of Pt concentration. The open circles are for disks A, open squares for disks B, closed circles for disks C, and closed squares for disks D. The a lattice parameter is shown in (a), while c is shown in (b). The closed triangles are taken from Ref. [15], which are for diffraction planes parallel to disk surfaces. All other data are for diffraction planes perpendicular to the disk surface. The solid line is a guide to the eye, while dashed and dot-dashed lines are lattice parameters calculated using Vegard's law and using an elastic model due to Friedel at low concentrations, respectively [28, 29]. It has been observed that there is a small dependence of the lattice parameters on media thickness [30] and B concentration [15]. Hence, these data have been normalized to an areal magnetization density (M_rT, where M_r is the remnant magnetization and T is the media thickness) of 0.2 and 10% B. The effect of this normalization is small.

Figure 5. Media fcc fraction and stacking fault probabilities as a function of Pt percentage. The symbols have the same meaning as in Fig. 4 and the line is a guide to the eye. Parts

(a), (b) and (c) are the total fcc fraction, the growth fault probability, and the deformation fault probability [26], respectively.

Figure 6. Media non-uniform strain (a) and the particle size (b) as a function of Pt percentage. The symbols have the same meaning as in Fig. 4.

Figure 7. High resolution TEM micrograph of CoPtCrB media (type C) with 32 % Pt.

Figure 8. Anisotropy field (H_k) as a function of Pt in the hcp CoPtCrB alloy (see text) for the CoPtCrB media (open symbols) and for bulk Co (filled circle). The line is a linear guide to the eye.

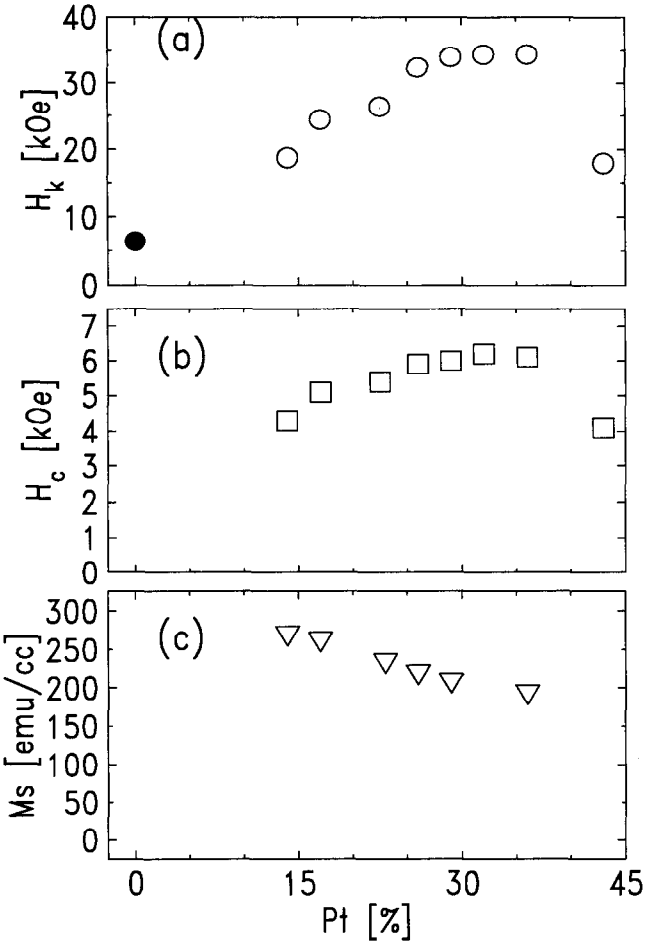

FIG. 1: Toney et al., JR03-1125

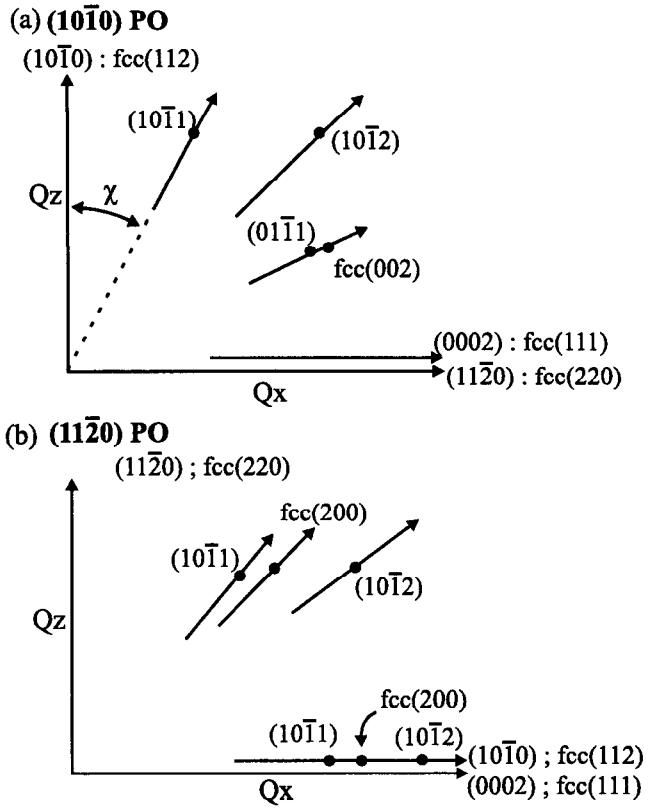

FIG. 2: Toney et al., JR03-1125

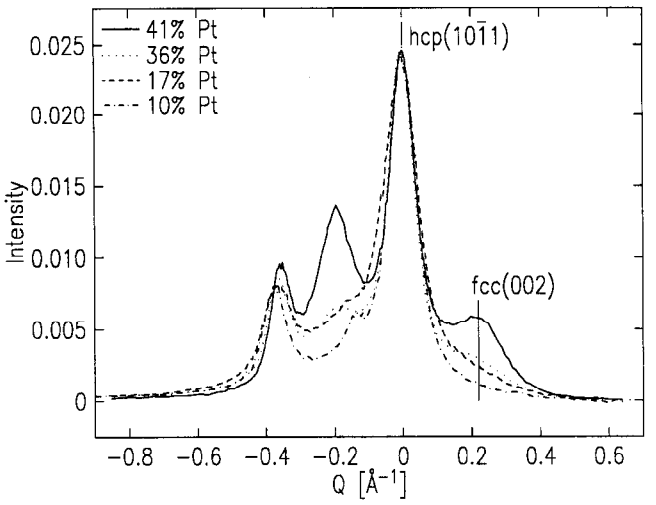

FIG. 3: Toney et al., JR03-1125

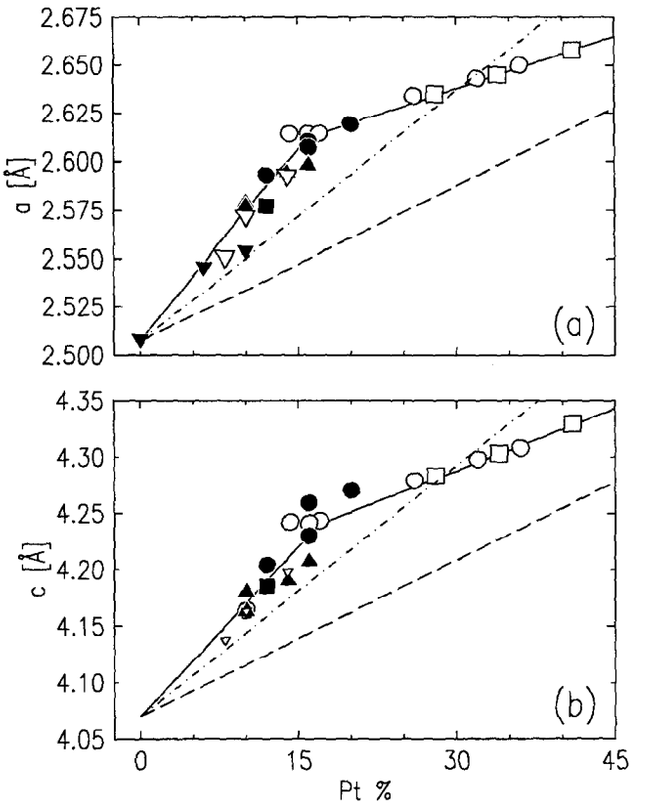

FIG. 4: Toney et al., JR03-1125

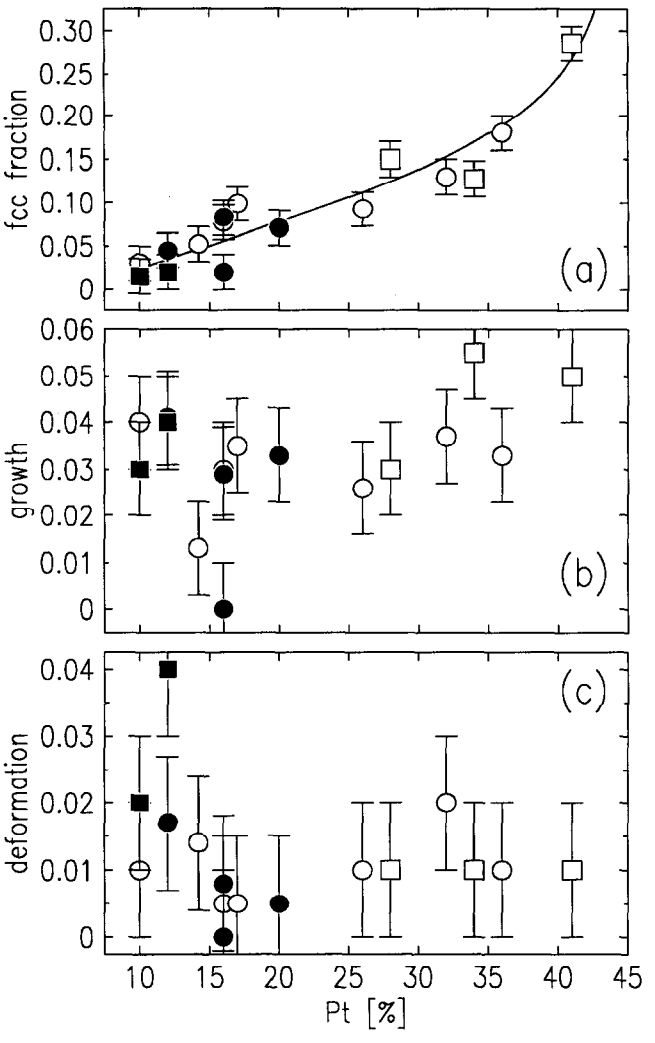

FIG. 5: Toney et al., JR03-1125

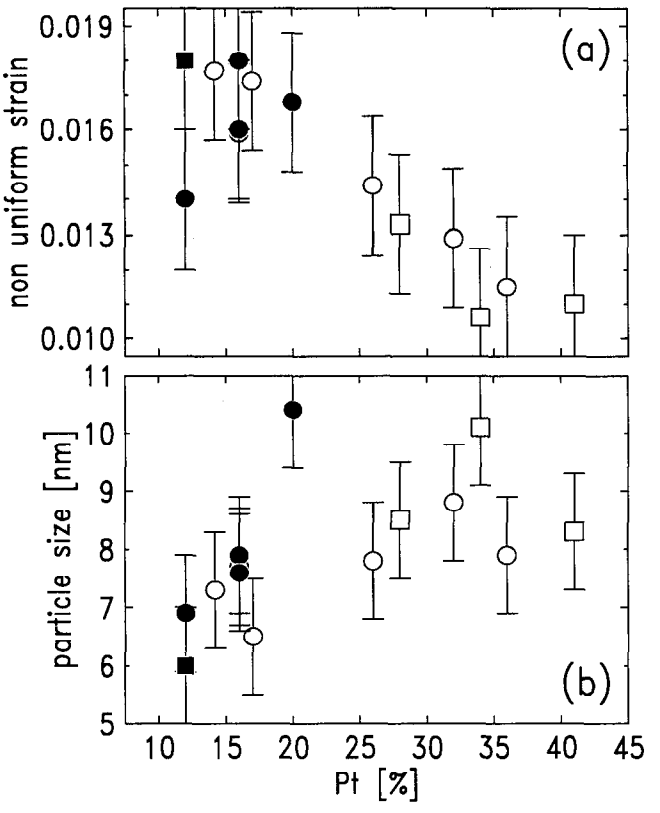

FIG. 6: Toney et al., JR03-1125

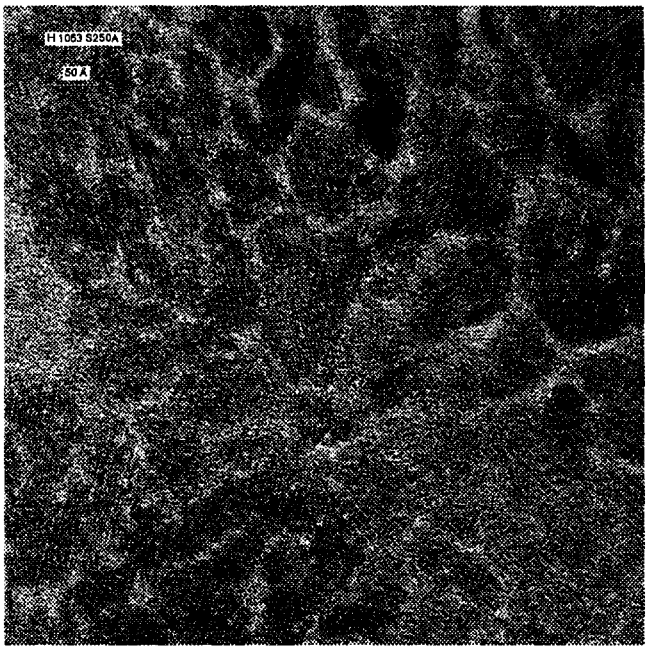

FIG. 7: Toney et al., JR03-1125

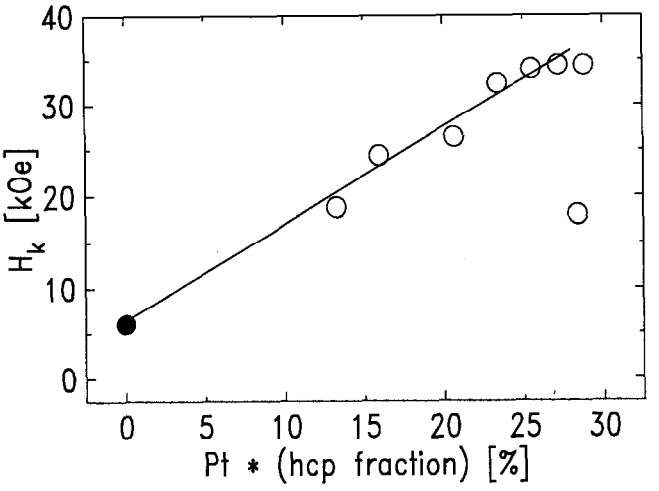

FIG. 8: Toney et al., JR03-1125